Nano Research

Open Access

Research Article

TiC-coated titanium foam via CVD as a 3D framework sulfur host for high-performance lithium–sulfur batteries

Jiahui Yuan[1,2], Wei Ding[1], Laxmi Raj Jaishi[1], Kasiviswanathan Muthukumarappan[2], Zhenqiang Wang[3], and Xiaojun Xian[1] ✉

[1] *The McComish Department of Electrical Engineering and Computer Science, Jerome J. Lohr College of Engineering, South Dakota State University, Brookings, South Dakota 57007, USA*
[2] *The Department of Agricultural and Biosystems Engineering, Jerome J. Lohr College of Engineering, South Dakota State University, Brookings, South Dakota 57007, USA*
[3] *The Department of Chemistry, The University of South Dakota, Vermillion, South Dakota 57069, USA*

Cite this article: *Nano Research*, **2025**, *18*, 94907828. https://doi.org/10.26599/NR.2025.94907828

ABSTRACT: Lithium–sulfur (Li–S) batteries are promising candidates for next-generation energy storage devices due to their high energy density, low cost, and environmental friendliness. However, their practical application remains limited by the polysulfide shuttle effect, sulfur volume expansion, and poor electronic conductivity of S and Li_2S. In this study, titanium carbide (TiC) was grown on Ti foam using chemical vapor deposition (CVD) to construct a binder-free, highly conductive, and porous TiC-Ti three-dimensional (3D) framework sulfur host for enhancing the Li–S battery performance. This 3D framework combines highly porous Ti foam with the polar surface of CVD-synthesized TiC nanoflowers, enabling efficient electron and ion transport, anchoring polysulfides to mitigate the shuttle effect, and accommodating sulfur volume expansion for enhanced cycling stability. Our study demonstrated that Li–S batteries utilizing TiC-Ti 3D framework@S cathodes achieved a high initial discharge capacity of 1506 mAh·g^{-1} at 0.1 C and maintained 93.3% of their capacity after 500 cycles at 1 C, with an exceptionally low average capacity decay of 0.01% per cycle. Additionally, the TiC-Ti 3D framework@S cathodes exhibited reduced charge transfer resistance after cycling, indicating enhanced interfacial reaction kinetics and stability. These findings confirm that the CVD-synthesized TiC-Ti 3D framework can serve as an efficient binder-free sulfur host, which provides a promising material and structural strategy for high-performance Li–S battery design.

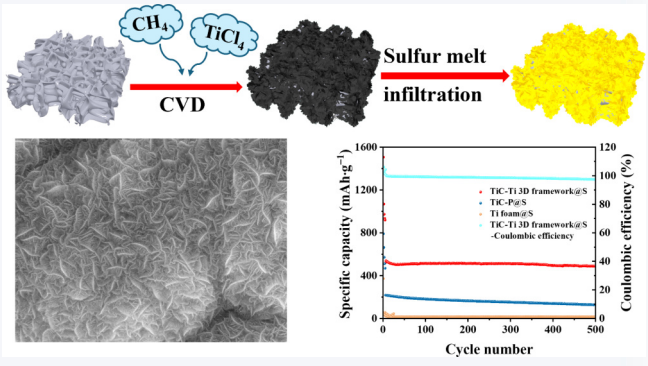

KEYWORDS: lithium–sulfur batteries, chemical vapor deposition (CVD), titanium foam, titanium carbide (TiC), three-dimensional (3D) framework, sulfur host

1 Introduction

The increasing demand for high-performance energy storage solutions across various industries, such as consumer electronics, electric vehicles, and renewable energy storage systems, has driven interest in advanced battery technologies [1–3]. Lithium–sulfur (Li–S) batteries, benefiting from the multi-electron redox conversion of sulfur, can offer a high theoretical capacity of 1675 mAh·g^{-1}, making them promising candidates for next-generation energy storage systems [3–5]. Additionally, sulfur is abundant, cost-effective, and environmentally friendly, further enhancing its potential for sustainable energy applications [6, 7]. However, the practical implementation of Li–S batteries in real-world applications faces several critical challenges, including the poor electrical conductivity of sulfur and its discharge products, substantial volume expansion during cycling, and the dissolution and migration of lithium polysulfides (Li_2S_n, $4 \le n \le 8$), known as the shuttle effect [8–10]. The shuttle effect leads to the irreversible loss of active material, electrode interface degradation, and side reactions, resulting in decreased Coulombic efficiency, accelerated capacity decay, and poor cycle life [11, 12]. These challenges severely hinder the commercialization of Li–S batteries.

Received: May 3, 2025; **Revised:** July 4, 2025
Accepted: July 22, 2025

✉Address correspondence to xiaojun.xian@sdstate.edu

The conventional slurry coating method for Li–S cathodes involves mixing sulfur with conductive agents (such as carbon black [13], graphene [14], and carbon nanotubes [15]) and binders, then applying it to a metal current collector. However, binders impede charge transport [16, 17], the current collector lacks volume buffering, and high shrinkage stress during drying can cause material detachment, leading to performance degradation and poor cycling stability [18–20]. To address these issues, porous conductive materials (such as porous carbon [21, 22] and metal foams [23, 24]) have been used as current collectors and effective sulfur hosts to provide strong sulfur adhesion and efficient electron/ion transport pathways [24–26], while eliminating the need for binders. Additionally, their intrinsic porosity accommodates volume expansion while physically confining polysulfides, thereby mitigating the shuttle effect and enhancing cycling stability and rate performance [21, 24, 27].

Titanium carbide (TiC) is an excellent candidate for sulfur hosting due to its high hardness (31.7 GPa) [28, 29], superior electrical conductivity (10^3–10^4 S·cm^{-1}) [30–32], and high melting point (3160 °C) [29, 33], along with its chemical stability [34, 35] and polysulfide anchoring capability [31, 36, 37]. Its polar surface can effectively immobilize polysulfides and catalyze sulfur redox conversion, thereby mitigating the shuttle effect [8, 38, 39], while its high electrical conductivity enables efficient mediation of rapid electron transfer and charge transport for electrochemical reactions. Various approaches have been employed to integrate TiC nanostructures into Li–S batteries, including the *in situ* reduction of TiO_2 nanofibers and the embedding of TiC nanoparticles [31, 39]. These strategies enhance polysulfide immobilization, reduce interfacial resistance, and improve sulfur utilization and rate capability. To further enhance the performance of Li–S batteries, TiC structures must be engineered to mitigate the volume expansion of the sulfur cathode during cycling. Chemical vapor deposition (CVD) provides a precise and controllable method for tailoring the nanostructure, crystallinity, and morphology of TiC [40, 41]. We propose that a well-designed three-dimensional (3D) TiC framework with a highly porous structure can serve as an efficient sulfur host, offering high electrical conductivity and structural resilience, ultimately enabling high-performance Li–S batteries.

In this study, TiC nanoflowers were uniformly grown on porous titanium foam (TF) via chemical vapor deposition to construct a fluffy, porous, and highly conductive 3D TiC framework, functioning as both a sulfur host and a binder-free current collector. The CVD process ensures uniform TiC growth, significantly increasing the specific surface area of the framework. The TiC-Ti 3D framework integrates the highly porous Ti foam with the polar surface of CVD-synthesized TiC nanoflowers, which effectively adsorb lithium polysulfides, mitigating the shuttle effect and enhancing sulfur utilization. Additionally, the 3D porous TiC-Ti 3D framework provides efficient electron/ion transport pathways and accommodates sulfur volume expansion during charge–discharge cycles, improving the structural stability of the electrode. Li–S batteries utilizing the TiC-Ti 3D framework@S cathode demonstrated an initial discharge capacity of 1506 mAh·g^{-1} at 0.1 C and retained 93.3% of their capacity after 500 cycles at 1 C, with an exceptionally low capacity decay of just 0.01% per cycle, showcasing excellent cycling stability. These results highlight the potential of CVD-synthesized TiC-Ti 3D framework as an efficient sulfur host, providing a promising strategy for high-performance Li–S battery development.

2 Experimental

2.1 Materials

Titanium foam (thickness: 0.25 mm, porosity: 50%–78%, and areal density: 100 mg·cm^{-2}) was purchased from TIBROMTACK, and $TiCl_4$ (99.6%) was purchased from Fisher Scientific. Aluminum foil (99.95%), lithium foil (99.9%), Super P conductive carbon black (acetylene black), polyvinylidene fluoride (PVDF) powder (99.5%), 1200 °C compact split tube furnace, and quartz tube were purchased from MTI Corp. Ar gas (ultra-high purity grade) and CH_4 (ultra-high purity grade) were purchased from Matheson Gas.

2.2 Synthesis of TiC-Ti 3D framework and TiC powder (TiC-P)

Before the experiment, the titanium foam was ultrasonically cleaned with acetone and ethanol to remove surface contaminants, followed by vacuum drying. A 1 cm × 1 cm piece of titanium foam was placed in an alumina boat, and then the alumina boat was placed into the quartz tube of a tube furnace. The CVD system was heated to 950 °C over 30 min under an argon flow rate of 120 sccm. Then Ar/$TiCl_4$ and CH_4 are introduced into the CVD system at flow rates of 120 and 5 sccm, respectively. After reacting at 950 °C for 1 h, the flow of CH_4 and $TiCl_4$ is stopped while maintaining an argon flow rate of 120 sccm. The tube furnace cover was opened to rapidly cool the system to room temperature, and the resulting TiC-Ti 3D framework was collected. The synthesis process of TiC-P followed a similar procedure to that of TiC-Ti 3D framework, with a 1 cm × 1 cm piece of titanium foil used as the raw material. The CVD reaction was conducted for 2 h to ensure complete reaction of the titanium foil.

2.3 Preparation of TiC-Ti 3D framework@S, TF@S, and TiC-P@S

0.5 g of sulfur was dissolved in 10 mL of toluene at 80 °C. Then, 100 μL of the sulfur-toluene solution was dropped-cast onto the TiC-Ti 3D framework substrate. After the complete evaporation of toluene, the sample was placed in an oven and subjected to molten infiltration at 155 °C for 12 h. After cooling, the TiC-Ti 3D framework@S was obtained. The synthesis procedure for TF@S was similar, except that the TiC-Ti 3D framework substrate was replaced with titanium foam. The sulfur loading was calculated by measuring the sample mass before and after sulfur infiltration. The sulfur loading of the TiC-Ti 3D framework@S is 2.0 mg·cm^{-2}.

TiC-P@S was prepared by sulfur impregnation of TiC-P using a molten diffusion method. Briefly, TiC-P and sulfur were mixed at a mass ratio of 1:3 and ground thoroughly. The mixture was then transferred to a sealed polytetrafluoroethylene (PTFE) container and heated at 155 °C for 12 h, yielding the TiC-P@S sample.

2.4 Material characterization

The morphologies of the samples were characterized by scanning electron microscopy (SEM, S-4700, FESEM, Hitachi). X-ray diffraction (XRD) patterns were recorded using a Rigaku SmartLab diffractometer. Surface composition was analyzed using X-ray photoelectron spectroscopy (XPS) on a ThermoFisher K-Alpha XPS/UPS photoelectron spectrometer, with all spectra calibrated to a C 1s peak at 284.8 eV. Nitrogen adsorption–desorption isotherms were acquired using Micromeritics analyzer (Micromeritics 3Flex) to calculate the specific surface area.

2.5 Electrochemical measurements

The electrochemical performances of the samples are evaluated in CR2032-type coin cells. The TiC-Ti 3D framework@S and TF@S were directly used as working electrodes. TiC-P@S working electrodes were made up of TiC-P@S, conducting carbon, and PVDF binder (the ratio of 7:2:1), formed with N-methyl-2-pyrrolidinone (NMP) solvent, coated on aluminum foil. The as-prepared working electrodes were dried in a vacuum oven at 80 °C for 12 h. Finally, the electrodes were cut into 12 mm circular disks. In lithium–sulfur batteries (Li–S), 16 mm commercial lithium foil acts as counter electrode, Celgard 2320 acts as separator, and 1.0 M lithium bis(trifluoromethanesulfonyl)imide (LiTFSI) in 1,2-dimethoxyethane (DME):1,3-dioxolane (DOL) = 1 vol%:1 vol% with 1.0% $LiNO_3$ acts as electrolyte. All cells were assembled in an argon-filled glovebox. The cycling and rate performance was tested on a battery test system (BTS, CT-4008, Neware, China) with a voltage ranging from 1.7 to 2.8 V. The cyclic voltammetry (CV) curves were recorded within a voltage window of 1.7–2.8 V at various scan rates using an electrochemical workstation (CHI-760E, Shanghai Chen Hua Instrument Co., Ltd.). The electrochemical impedance spectroscopy (EIS) was performed at a frequency ranging from 0.01 Hz to 100 kHz using CHI-760E electrochemical workstation. All measurements were conducted at room temperature.

2.6 Adsorption test of lithium polysulfides

The Li_2S_6 solution was prepared by dissolving sulfur and Li_2S in a molar ratio of 5:1 within a DOL/DME (1:1, v/v) solvent system at 60 °C for 24 h. Before the adsorption tests, all samples (TiC-Ti 3D framework, TF, and TiC-P) were dried in a vacuum oven at 80 °C for 12 h. Subsequently, the dried samples were immersed in a 2 mM Li_2S_6 solution (5 mL) and stored under argon atmosphere for 24 h in a glove box. The supernatants were then collected for ultraviolet–visible (UV–vis) absorption spectroscopy analysis.

3 Results and discussion

Figure 1(a) schematically illustrates the CVD process for synthesizing TiC-Ti 3D framework, followed by the sulfur loading process. In this method, CH_4 served as the carbon source, while gaseous $TiCl_4$ and Ti foam acted as titanium sources. Additionally, the Ti foam also served as the deposition substrate for TiC growth. During the typical CVD synthesis, the system was gradually heated to 950 °C. Due to the high volatility of liquid $TiCl_4$, argon was used as a carrier gas to transport $TiCl_4$ vapor into the reaction chamber, where it reacted with CH_4, leading to the uniform deposition of TiC on the Ti foam within 1 h. The entire reaction process was conducted under an inert Ar atmosphere. After synthesizing TiC-Ti 3D framework, sulfur was loaded into its porous framework

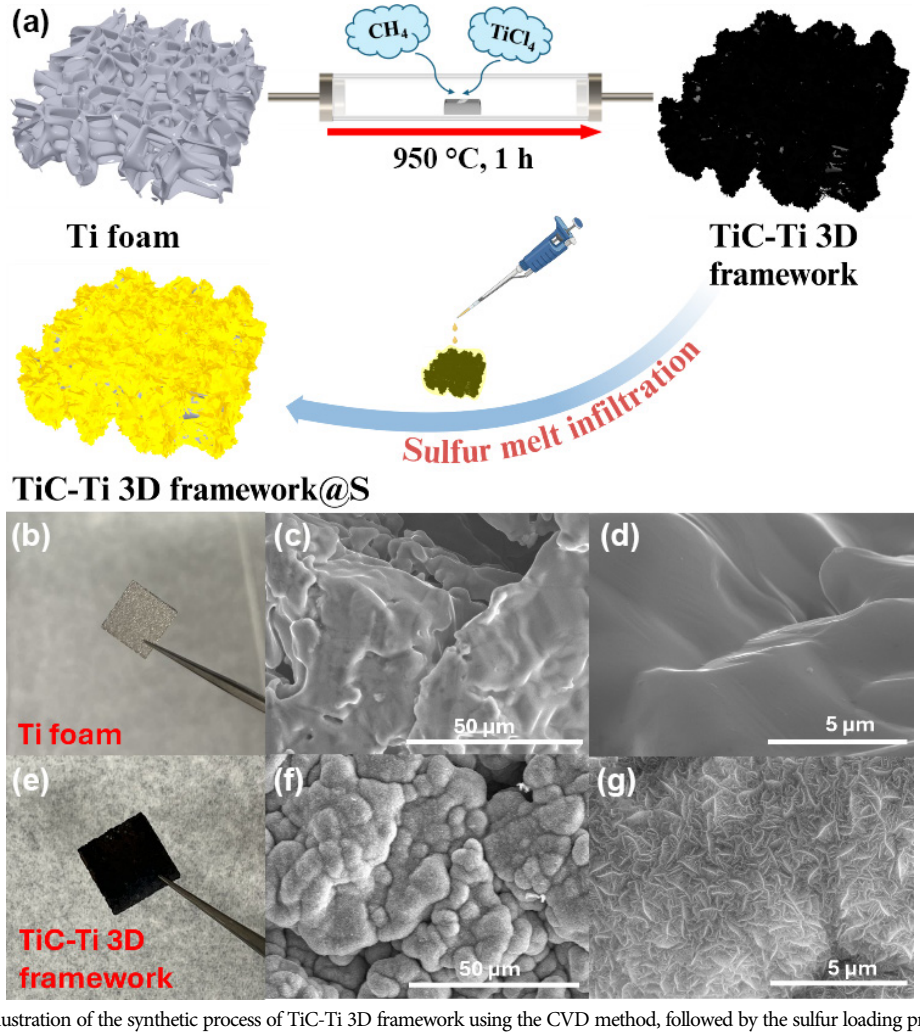

Figure 1 (a) Schematic illustration of the synthetic process of TiC-Ti 3D framework using the CVD method, followed by the sulfur loading process. (b) Digital image of Ti foam. ((c) and (d)) SEM images of Ti foam. (e) Digital image of TiC-Ti 3D framework. ((f) and (g)) SEM images of TiC-Ti 3D framework.

through a molten infiltration process. A sulfur-toluene solution was drop-cast onto the TiC-Ti 3D framework substrate and dried to remove the solvent. A sulfur-toluene solution was drop-cast onto the TiC-Ti 3D framework substrate and dried to remove the solvent. After cooling, the sulfur-loaded TiC-Ti 3D framework@S was obtained. The well-controlled CVD-grown TiC layer with a nanoflower structure on Ti foam provides a high surface area, highly conductive, and mechanically robust scaffold that ensures uniform sulfur distribution and mitigates volume expansion. Its porous structure provides abundant sites for polysulfide immobilization, effectively suppressing the shuttle effect. The combination of these structural and chemical advantages enhances the electrochemical stability and cycling performance of Li–S batteries.

The morphologies of Ti foam before and after TiC growth were characterized using SEM. As shown in the digital images (Figs. 1(b) and 1(e)), the pristine Ti foam exhibits a smooth, porous structure with a metallic silver luster. After TiC growth, the surface becomes fluffy and rough, covered with a black TiC layer. The SEM images reveal the smooth and porous structure of the pristine Ti foam (Figs. 1(c) and 1(d)). In contrast, the CVD process induces the formation of a dense, fluffy nanoflower-like TiC morphology, composed of stacked nanosheets uniformly deposited on the surface of the Ti foam (Figs. 1(f) and 1(g)). Furthermore, cross-sectional SEM images (Fig. S1 in the Electronic Supplementary Material (ESM)) confirm that the TiC nanoflower layer is uniformly coated not only on the external surface but also along the internal pore walls of the Ti foam, with a coating thickness of approximately 8.9 μm.

Figure 2(a) is the energy dispersive spectroscopy (EDS) elemental mapping of TiC-Ti 3D framework, confirming the uniform distribution of Ti, C, and Cl on the sample surface. The presence of Cl is attributed to residual $TiCl_4$ precursor from the synthesis process. Additionally, elemental composition analysis from EDS (Fig. S2 in the ESM) shows a Ti/C ratio close to 1:1, further indicating the uniform growth and coverage of TiC on the Ti foam surface.

Traditional CVD methods use $TiCl_4$ as the titanium source to deposit TiC films on graphite or metal substrates via a gas-phase reaction [42, 43], which may result in weak interfacial adhesion between the TiC layer and the substrate. In contrast, our method utilizes both $TiCl_4$ and Ti foam as titanium sources. It was reported that Ti will react with CH_4 via a gas–solid chemical reaction at temperatures above 700 °C [40, 41, 44], enabling the *in situ* growth of TiC on the Ti substrate. The combination of two TiC synthesis reactions ensures strong interfacial bonding, enhances mechanical stability, and prevents the shedding of TiC during cycling. This robust adhesion improves the structural durability and electrochemical performance of TiC-Ti 3D framework, making it a more stable and binder-free sulfur host for Li–S batteries.

The elemental composition and chemical states of TiC-Ti 3D framework were analyzed using XPS. The survey spectrum (Fig. S3(a) in the ESM) confirms the presence of Ti, C, and Cl, consistent with the EDS results. The high-resolution Ti 2p spectrum (Fig. 2(b)) exhibits binding energy peaks at ~ 455.0, ~ 456.7, and ~ 461.1 eV, corresponding to Ti–C bonds [45], confirming the successful formation of TiC on Ti foam. A peak at ~ 455.7 eV is attributed to Ti–O bonds, likely caused by surface oxidation, while the peak at ~ 458.9 eV is assigned to Ti^0 ($2p_{1/2}$) [40]. The C 1s spectrum (Fig. 2(c)) displays binding energy peaks at ~ 282.1, ~ 284.8, and ~ 286.0 eV, corresponding to C–Ti, C–C, and C–O bonds, respectively [46]. Additionally, the Cl 2p spectrum (Fig. S3(b) in the ESM) shows peaks at ~ 199.3 and ~ 201.0 eV, associated with Cl–Ti and Cl–C bonds [40]. Raman spectroscopy was performed on TiC-Ti 3D framework and TiC-P (Fig. 2(d)). Both samples exhibited three distinct peaks at 608.5, 419.3, and 260.0 cm^{-1}, which

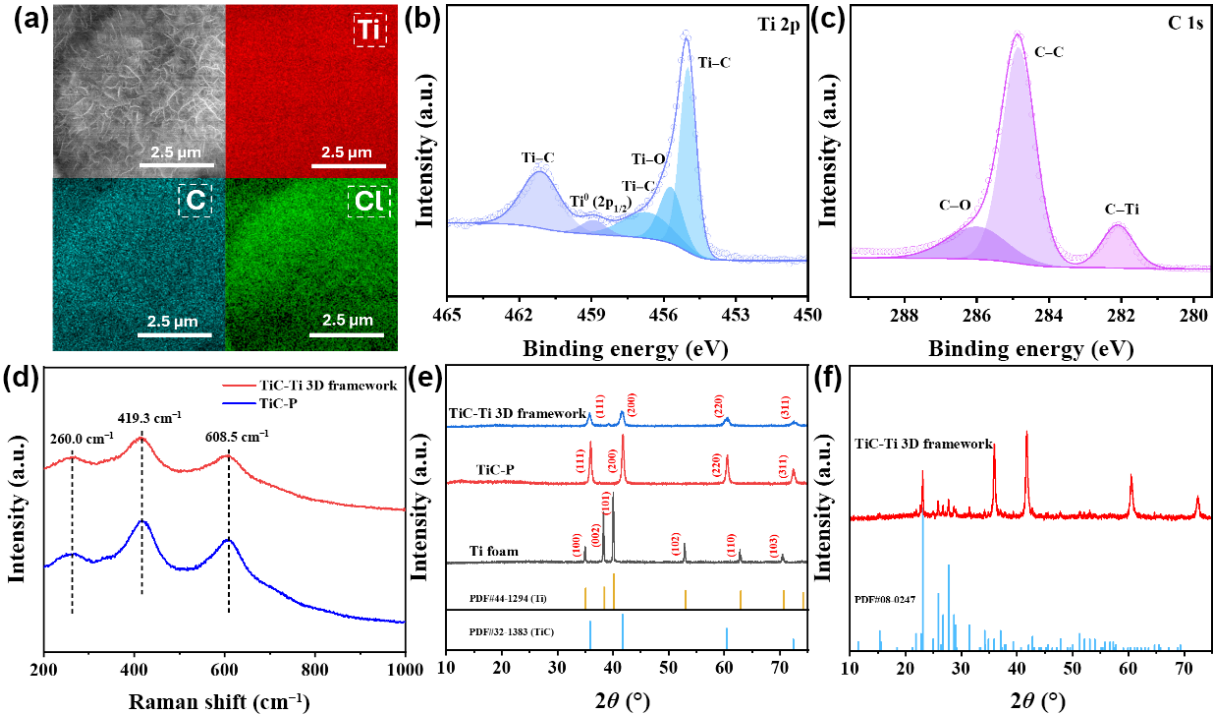

Figure 2 (a) SEM and EDS mapping images of Ti, C, and Cl for TiC-Ti 3D framework. ((b) and (c)) High-resolution XPS spectra of Ti 2p and C 1s of TiC-Ti 3D framework. (d) Raman spectra of TiC-Ti 3D framework and TiC-P. (e) XRD spectra of TiC-Ti 3D framework, TiC-P, and Ti foam. (f) XRD spectrum of TiC-Ti 3D framework@S.

correspond to the characteristic Raman scattering signals of TiC [40, 47]. According to the Brunauer–Emmett–Teller (BET) analysis results (Fig. S4 in the ESM), the Ti foam exhibits a negligible specific surface area, whereas the TiC-Ti 3D framework shows a significantly increased surface area of 11.0 $m^2 \cdot g^{-1}$, comparable to other porous TiC nanostructures [31, 48, 49]. This improvement is attributed to the surface coverage by TiC nanoflowers, which introduces porous structures within the framework. Such hierarchical porosity not only facilitates electrolyte infiltration and ion transport but also physically confines lithium polysulfides, effectively suppressing the shuttle effect, contributing to the enhanced electrochemical performance of the Li–S batteries.

The XRD patterns of TiC-Ti 3D framework, TiC-P, and Ti foam are shown in Fig. 2(e). The Ti foam exhibits characteristic peaks at (100), (002), (101), (102), (110), and (103), while TiC-Ti 3D framework and TiC-P show (111), (200), (220), and (311) peaks, matching the cubic TiC structure (PDF#32-1383) [40] and confirming successful synthesis of TiC. Weak characteristic peaks of Ti foam remain visible in the XRD pattern of TiC-Ti 3D framework, indicating the retention of the original Ti framework. Figure 2(f) shows the XRD pattern of TiC-Ti 3D framework@S, revealing distinct elemental sulfur (S_8) peaks [22] alongside TiC characteristic peaks. The peaks align with the standard S_8 pattern (PDF#08-0247), confirming successful sulfur loading onto the TiC-Ti 3D framework. Furthermore, cross-sectional EDS mapping (Fig. S5 in the ESM) demonstrates that sulfur is uniformly distributed throughout the internal structure of the TiC-Ti 3D framework after the melt infiltration process, indicating that sulfur can effectively infiltrate into the 3D framework.

The TiC-Ti 3D framework@S was used as cathode and lithium foil as the anode to assemble CR2032 coin cells for electrochemical performance evaluation. The galvanostatic charge–discharge (GCD) test results for TiC-Ti 3D framework@S and TiC-P@S are shown in Fig. 3(a) and Fig. S6 in the ESM, respectively. Both samples exhibited typical charge–discharge plateaus at 2.3 and 2.1 V, corresponding to the reduction of S_8 to long-chain polysulfides (Li_2S_n, $4 < n < 8$) and further reduction to Li_2S_2 and Li_2S [22]. To further investigate the sulfur conversion mechanism, XPS analysis of sulfur species at different electrochemical states was conducted (Fig. S7 in the ESM). The results confirm the reversible conversion between S_8 and Li_2S during cycling, providing direct evidence for the redox process and supporting the observed electrochemical behavior. Besides, TiC-Ti 3D framework@S demonstrated a higher initial discharge capacity of 1506 $mAh \cdot g^{-1}$, compared to 902 $mAh \cdot g^{-1}$ for TiC-P@S, indicating its enhanced sulfur utilization. Figure 3(b) presents the CV curves of TiC-Ti 3D framework@S for the first three cycles at a scan rate of 0.05 $mV \cdot s^{-1}$. After the initial scan (indicating the formation of solid electrolyte interface (SEI)), the overlapping CV curves of the second and third cycles indicate the effective lithium polysulfide capture and excellent electrochemical stability of TiC-Ti 3D framework@S. The reduction peaks at 2.25 and 1.89 V indicate the stepwise conversion of S_8 to Li_2S_2 and Li_2S, while the broad continuous oxidation peaks around 2.52 V correspond to their reoxidation into long-chain polysulfides and ultimately to S_8 [18, 50].

The rate performance of TiC-Ti 3D framework@S and TiC-P@S was evaluated at current densities from 0.1 to 2 C (Fig. 3(c)). TiC-Ti 3D framework@S exhibited discharge capacities of 935.92, 838.86, 679.17, 487.41, and 313.91 $mAh \cdot g^{-1}$ at 0.1, 0.2, 0.5, 1, and 2 C, respectively, whereas TiC-P@S delivered lower capacities of 410.32, 318.66, 264.05, 222.51, and 185.33 $mAh \cdot g^{-1}$. Notably, when the current density returned to 0.1 C, TiC-Ti 3D framework@S regained 876.69 $mAh \cdot g^{-1}$ (93.7% retention), while TiC-P@S recovered only 271.79 $mAh \cdot g^{-1}$ (66.1% retention). These results demonstrate the superior rate capability of TiC-Ti 3D framework@S and its excellent structural stability even after cycling at high current densities.

EIS tests of TiC-Ti 3D framework@S were performed before and after cycling (Fig. 3(d)), with the equivalent circuit shown in Fig. S8 in the ESM. After cycling, TiC-Ti 3D framework@S showed a

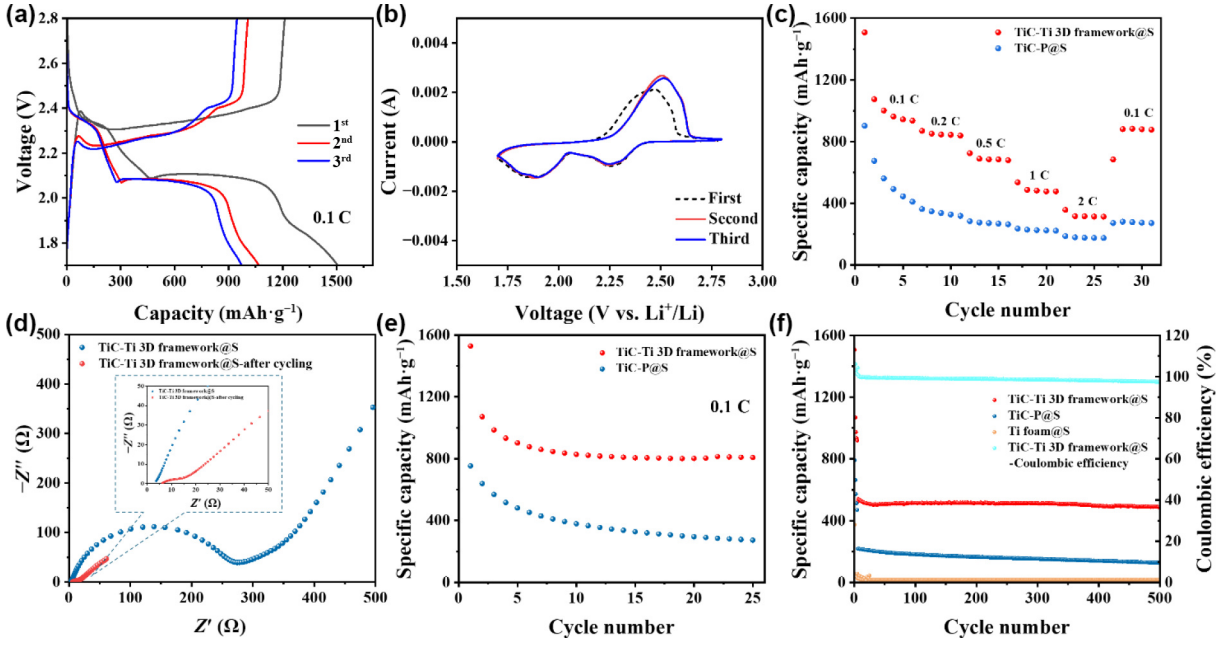

Figure 3 (a) Galvanostatic charge–discharge tests of TiC-Ti 3D framework@S at 0.1 C. (b) First three CV cycle curves of TiC-Ti 3D framework@S. (c) Rate performance of TiC-Ti 3D framework@S and TiC-P@S. (d) Nyquist plots of TiC-Ti 3D framework@S before and after 50 cycles. (e) Cycling performance at a current density of 0.1 C of TiC-Ti 3D framework@S and TiC-P@S. (f) Cycling performance at a current density of 1 C of TiC-Ti 3D framework@S, TiC-P@S, and Ti foam@S.

significant reduction in charge transfer resistance (R_{ct}), decreasing from 233.2 to 9.9 Ω (Table S1 in the ESM), which indicates improved interfacial reaction kinetics. This improvement confirms that TiC-Ti 3D framework@S maintains excellent electrochemical performance while enhancing interfacial reaction dynamics, validating its feasibility as a lithium–sulfur cathode.

The cycling performance at 0.1 C (Fig. 3(e)) shows that TiC-Ti 3D framework@S exhibits a higher initial capacity and better retention than TiC-P@S. The rapid capacity decay of TiC-P@S indicates insufficient polysulfide confinement, while the stable capacity of TiC-Ti 3D framework@S reflects improved sulfur utilization and structural stability. To further investigate the stability of TiC-Ti 3D framework@S as a lithium–sulfur battery cathode, its long-term cycling performance was evaluated at a high current density of 1 C (Fig. 3(f)). After activation at 0.1 C, the initial discharge capacities at 1 C for TiC-Ti 3D framework@S, TiC-P@S, and Ti foam@S were 523, 218, and 23 mAh·g^{-1}, respectively. The slight capacity drop observed during the early cycles is mainly due to the increased current density after activation and the irreversible loss of active material from polysulfide dissolution. Despite this initial decline, the battery exhibits excellent capacity retention and stable cycling performance in the subsequent cycles, indicating improved interfacial stability and enhanced redox reversibility. After 500 cycles at 1 C, TiC-Ti 3D framework@S retained 488 mAh·g^{-1} with 93.3% capacity retention and an average decay of just 0.01% per cycle, while maintaining a Coulombic efficiency above 97%. In contrast, TiC-P@S retained only 126 mAh·g^{-1} after 500 cycles (57.8% retention). Ti foam@S showed negligible capacity, demonstrating the superior cycling stability of TiC-Ti 3D framework@S even at high rates. Compared to materials reported in relevant references (Table S2 in the ESM), the TiC-Ti 3D framework@S demonstrates competitive capacity, cycling stability, and long-term retention performance. Furthermore, the charge–discharge curves of TiC-Ti 3D framework@S remained highly consistent after 500 cycles at 1 C (Fig. S9 in the ESM). Under high sulfur loading (5 mg·cm^{-2}), the TiC-Ti 3D framework@S electrode still exhibits good cycling stability, maintaining 360 mAh·g^{-1} with 80% capacity retention after 500 cycles at 1 C (Fig. S10 in the ESM). This superior stability stems from the structural advantages of TiC-Ti 3D framework, where the porous TiC nanoflowers accommodate sulfur expansion and maintain electrode integrity. The interconnected porosity of Ti foam alleviates stress, prevents structural collapse, and preserves contact between the active material and conductive framework, ensuring long-term electrochemical stability.

To investigate the structural changes of the electrodes after long-term cycling, SEM analysis was conducted on TiC-Ti 3D framework@S and TiC-P@S before and after 500 cycles. As shown in Figs. 4(a) and 4(b), TiC-Ti 3D framework@S maintained its porous TiC nanoflower structure after long-term cycling. XRD analysis (Fig. S11 in the ESM) further confirms that the surface crystallization in Fig. 4(b) is due to the re-deposition of S_8 during charging, consistent with the sulfur signal in Fig. 2(f). The SEM image (Fig. S12(a) in the ESM) and EDS mapping (Fig. S12(b) in the ESM) of TiC-Ti 3D framework@S charged to 2.8 V confirm uniform sulfur distribution within the TiC nanoflowers, indicating effective sulfur confinement. In contrast, TiC-P@S exhibits significant aggregation and structural collapse, with reduced porosity and surface cracks (Figs. S13(a) and S13(b) in the ESM). Additionally, compared to Fig. S13(c) in the ESM, digital images (Figs. S13(d) and S13(e) in the ESM) reveal severe wrinkling and delamination of the TiC-P@S electrode, likely due to volume expansion of sulfur, causing material deformation and detachment from the current collector, leading to performance degradation. Although a higher binder content could mitigate this issue, it would also cover more active sites, negatively impacting electrochemical

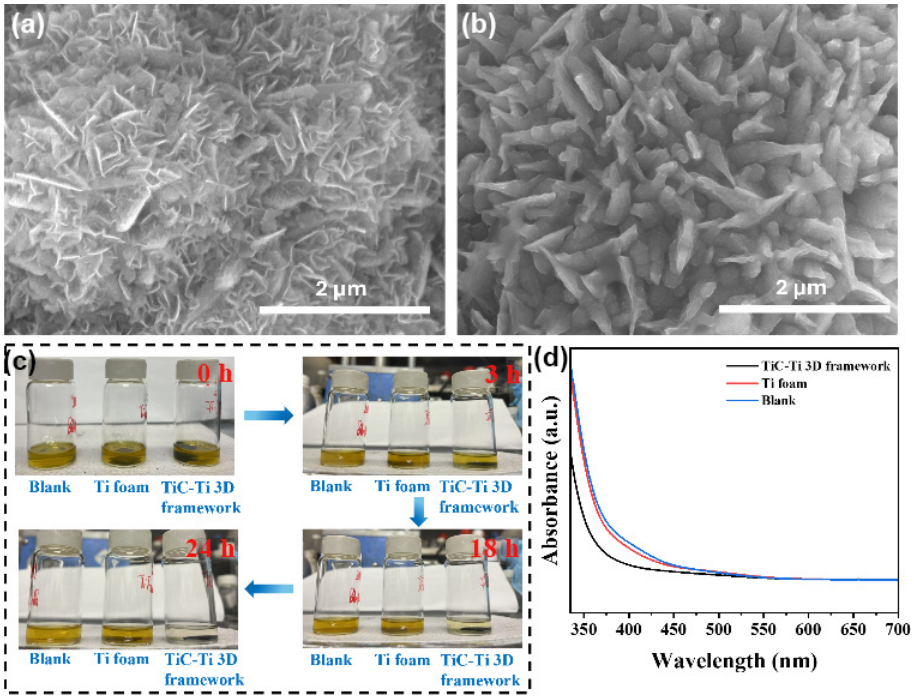

Figure 4 ((a) and (b)) SEM images of TiC-Ti 3D framework@S before cycling (a) and after 500 cycles (b) at 1 C for Li–S batteries. ((c) and (d)) Adsorption test of lithium polysulfides: (c) digital images of Li_2S_6 solution after adsorption by TiC-Ti 3D framework and Ti foam and (d) UV–vis spectra of Li_2S_6 solution after adsorption by TiC-Ti 3D framework and Ti foam.

performance. For the binder-free TiC-Ti 3D framework@S, it maintained its structural integrity after long-term cycling, with the TiC nanoflowers remaining tightly attached to the Ti foam surface without delamination (Fig. S14 in the ESM). These findings demonstrate that the nanoflower TiC structure, coupled with the robust Ti foam framework, effectively accommodates sulfur volume expansion and preserves electrode integrity.

To verify the adsorption effect of TiC-Ti 3D framework for lithium polysulfides, we investigated the adsorption behavior of TiC-Ti 3D framework and Ti foam toward Li_2S_6 [18, 51]. Three vials were prepared, each containing 5 mL of a 2 mM Li_2S_6 solution. The first vial served as a blank control with no additional material, while Ti foam and TiC-Ti 3D framework were added to the second and third vials, respectively, and all were placed in an argon-filled glovebox. The color change of the solutions over time was visually monitored to evaluate the adsorption performance. As shown in Fig. 4(c), the solution with TiC-Ti 3D framework gradually lightened over time and turned completely clear after 24 h, indicating effective polysulfide adsorption. In contrast, no significant color change was observed in the blank solution or the solution with Ti foam. These results confirmed the strong adsorption capability of TiC-Ti 3D framework for lithium polysulfides. The UV–vis spectra of the Li_2S_6 solutions after adsorption are shown in Fig. 4(d). The characteristic absorption peaks observed in the range of 350–550 nm are attributed to polysulfides. Compared to the blank control, the solution containing Ti foam showed a slight absorbance decrease, while the solution with TiC-Ti 3D framework exhibited a significant reduction, indicating superior adsorption capacity [18, 51]. This result further confirms TiC-Ti 3D framework's effectiveness as a sulfur cathode host, efficiently adsorbing lithium polysulfides and suppressing the shuttle effect.

4 Conclusions

In this study, TiC nanoflowers were uniformly grown on Ti foam using CVD to construct a binder-free, highly conductive, and porous TiC-Ti 3D framework sulfur host. The polar surface of TiC effectively anchors lithium polysulfides, suppressing the shuttle effect and enhancing sulfur utilization. The nanoflower-like TiC structure, combined with the 3D porous framework of Ti foam, provides efficient electron/ion transport pathways while buffering volume expansion during charge–discharge cycles, thereby improving electrode structural stability and cycling lifespan. Electrochemical tests demonstrated that TiC-Ti 3D framework@S achieved an initial discharge capacity of 1506 mAh·g^{-1} at 0.1 C and retained 93.3% of its capacity after 500 cycles at 1 C, with an average capacity decay of only 0.01% per cycle. Additionally, TiC-Ti 3D framework@S exhibited lower charge transfer resistance after cycling, indicating enhanced interfacial reaction kinetics, which further improved its rate performance and cycling stability. This study demonstrates the benefits of the CVD-synthesized TiC-Ti 3D framework in suppressing the shuttle effect, enhancing sulfur utilization, and improving electrode structural stability. These findings present a promising material and structural strategy for high-performance Li–S batteries and provide valuable insights for the future design and optimization of sulfur cathode materials.

Electronic Supplementary Material: Supplementary material (EDS, XPS, BET, GCD, and SEM test results) is available in the online version of this article at https://doi.org/10.26599/NR.2025.94907828.

Data availability

All data needed to support the conclusions in the paper are presented in the manuscript and the Electronic Supplementary Material. Additional data related to this paper may be requested from the corresponding author upon request.

Acknowledgements

The authors thank the startup fund from the Department of Electrical Engineering and Computer Science at South Dakota State University for supporting this research.

Declaration of competing interest

All the contributing authors report no conflict of interests in this work.

Author contribution statement

J. H. Y.: Writing – original draft, data curation, investigation, methodology, validation, visualization. W. D.: Methodology, validation, visualization. L. R. J.: Methodology, visualization. K. M.: Validation. Z. Q. W.: Resources, validation. X. J. X.: Writing – review & editing, data curation, investigation, methodology, validation, visualization. All the authors have approved the final manuscript.

Use of AI statement

None.

References

[1] Chen, Y.; Wang, T. Y.; Tian, H. J.; Su, D. W.; Zhang, Q.; Wang, G. X. Advances in lithium–sulfur batteries: From academic research to commercial viability. *Adv. Mater.* **2021**, *33*, 2003666.

[2] Bi, C. X.; Hou, L. P.; Li, Z.; Zhao, M.; Zhang, X. Q.; Li, B. Q.; Zhang, Q.; Huang, J. Q. Protecting lithium metal anodes in lithium–sulfur batteries: A review. *Energy Mater. Adv.* **2023**, *4*, 0010.

[3] Pei, F.; Lin, L. L.; Ou, D. H.; Zheng, Z. M.; Mo, S. G.; Fang, X. L.; Zheng, N. F. Self-supporting sulfur cathodes enabled by two-dimensional carbon yolk–shell nanosheets for high-energy-density lithium–sulfur batteries. *Nat. Commun.* **2017**, *8*, 482.

[4] Li, Z. N.; Sami, I.; Yang, J.; Li, J. T.; Kumar, R. V.; Chhowalla, M. Lithiated metallic molybdenum disulfide nanosheets for high-performance lithium–sulfur batteries. *Nat. Energy* **2023**, *8*, 84–93.

[5] Qi, X. D.; Zhang, C. Y.; Yu, J.; Huang, C.; Yu, A.; Xue, Q.; Li, C. H.; Li, K.; Lu, X.; Ren, Y. C. et al. Rapid electron transfer in $Co_{0.85}Se$-$MoSe_2$/NCP heterostructure catalyst towards robust lithium–sulfur batteries. *J. Energy Chem.* **2025**, *106*, 852–863.

[6] Li, L.; Nam, J. S.; Kim, M. S.; Wang, Y. F.; Jiang, S. H.; Hou, H. Q.; Kim, I. D. Sulfur-carbon electrode with PEO-LiFSI-PVDF composite coating for high-rate and long-life lithium–sulfur batteries. *Adv. Energy Mater.* **2023**, *13*, 2302139.

[7] Nakamura, N.; Ahn, S.; Momma, T.; Osaka, T. Future potential for lithium–sulfur batteries. *J. Power Sources* **2023**, *558*, 232566.

[8] Huang, Y. Z.; Lin, L.; Zhang, C. K.; Liu, L.; Li, Y. K.; Qiao, Z. S.; Lin, J.; Wei, Q. L.; Wang, L. S.; Xie, Q. S. et al. Recent advances and strategies toward polysulfides shuttle inhibition for high-performance Li–S batteries. *Adv. Sci.* **2022**, *9*, 2106004.

[9] Shen, Z. H.; Jin, X.; Tian, J. M.; Li, M.; Yuan, Y. F.; Zhang, S.; Fang, S. S.; Fan, X.; Xu, W. G.; Lu, H. et al. Cation-doped ZnS catalysts for polysulfide conversion in lithium–sulfur batteries. *Nat. Catal.* **2022**, *5*, 555–563.

[10] Chen, M.; Shao, M. M.; Jin, J. T.; Cui, L. F.; Tu, H. R.; Fu, X. W. Configurational and structural design of separators toward shuttling-free and dendrite-free lithium–sulfur batteries: A review. *Energy Storage Mater.* **2022**, *47*, 629–648.

[11] Wang, M. Y.; Bai, Z. C.; Yang, T.; Nie, C. H.; Xu, X.; Wang, Y. X.; Yang, J.; Dou, S. X.; Wang, N. N. Advances in high sulfur loading cathodes for practical lithium–sulfur batteries. *Adv. Energy Mater.* **2022**, *12*, 2201585.

[12] Zhang, H.; Zhang, M. T.; Liu, R. Y.; He, T. F.; Xiang, L. X.; Wu, X. R.; Piao, Z. H.; Jia, Y. Y.; Zhang, C. Y.; Li, H. et al. Fe_3O_4-doped mesoporous carbon cathode with a plumber's nightmare structure for high-performance Li–S batteries. *Nat. Commun.* **2024**, *15*, 5451.

[13] Li, J.; Xie, F. X.; Pang, W. W.; Liang, Q. Y.; Yang, X. F.; Zhang, L. Regulate transportation of ions and polysulfides in all-solid-state Li–S batteries using ordered-MOF composite solid electrolyte. *Sci. Adv.* **2024**, *10*, eadl3925.

[14] Han, D. D.; Wang, Z. Y.; Pan, G. L.; Gao, X. P. Metal–organic-framework-based gel polymer electrolyte with immobilized anions to stabilize a lithium anode for a quasi-solid-state lithium–sulfur battery. *ACS Appl. Mater. Interfaces* **2019**, *11*, 18427–18435.

[15] Cheng, X. B.; Huang, J. Q.; Zhang, Q.; Peng, H. J.; Zhao, M. Q.; Wei, F. Aligned carbon nanotube/sulfur composite cathodes with high sulfur content for lithium–sulfur batteries. *Nano Energy* **2014**, *4*, 65–72.

[16] Guo, R. N.; Yang, Y.; Huang, X. L.; Zhao, C. C.; Hu, B. B.; Huo, F.; Liu, H. K.; Sun, B. W.; Sun, Z. X.; Dou, S. X. Recent advances in multifunctional binders for high sulfur loading lithium–sulfur batteries. *Adv. Funct. Mater.* **2024**, *34*, 2307108.

[17] Li, Z. H.; Wu, G.; Yang, Y. J.; Wan, Z. W.; Zeng, X. M.; Yan, L. J.; Wu, S. X.; Ling, M.; Liang, C. D.; Hui, K. N. et al. An ion-conductive grafted polymeric binder with practical loading for silicon anode with high interfacial stability in lithium-ion batteries. *Adv. Energy Mater.* **2022**, *12*, 2201197.

[18] Wang, N. N.; Zhang, X.; Ju, Z. Y.; Yu, X. W.; Wang, Y. X.; Du, Y.; Bai, Z. C.; Dou, S. X.; Yu, G. H. Thickness-independent scalable high-performance Li–S batteries with high areal sulfur loading via electron-enriched carbon framework. *Nat. Commun.* **2021**, *12*, 4519.

[19] Luo, Y. F.; Wang, L.; Wei, Z. Y.; Huang, Q. Y.; Deng, Y. H.; Zheng, Z. J. Cracking-controlled slurry coating of mosaic electrode for flexible and high-performance lithium–sulfur battery. *Adv. Energy Mater.* **2023**, *13*, 2203621.

[20] Zeng, F. L.; Zhou, X. Y.; Li, N.; Wang, A. B.; Wang, W. K.; Jin, Z. Q.; Ren, Y. R.; Fang, B. J.; Yuan, N. Y.; Ding, J. N. A multifunctional zipper-like sulfur electrode enables the stable operation of lithium–sulfur battery through self-healing chemistry. *Energy Storage Mater.* **2021**, *34*, 755–767.

[21] Hu, H.; Cui, L. F.; Gao, W. K.; Zhang, Z. Y.; Kang, S. F. Unraveling the hierarchical porous structure in natural pollen-derived Fe-containing carbon to address the shuttle effect and dead sulfur problems in lithium–sulfur batteries. *Chem. Eng. J.* **2023**, *453*, 139516.

[22] Guo, Y. C.; Khatoon, R.; Lu, J. G.; He, Q. G.; Gao, X.; Yang, X. P.; Hu, X.; Wu, Y.; Lian, J. L.; Li, Z. P. et al. Regulating adsorption ability toward polysulfides in a porous carbon/Cu_3P hybrid for an ultrastable high-temperature lithium–sulfur battery. *Carbon Energy* **2021**, *3*, 841–855.

[23] Zhou, Q. Y.; Tan, L.; Lv, T. B.; Li, M. C.; Zhang, J. J.; Zhao, Z. Q.; Jin, X. J.; Liu, Z.; Hou, P. P.; Zeng, Z. L. et al. Nickel foam coated by Ni nanoparticle-decorated 3D nanocarbons as a freestanding host for high-performance lithium–sulfur batteries. *ACS Appl. Mater. Interfaces* **2023**, *15*, 3037–3046.

[24] Sörgel, Ş.; Kesten, O.; Wengel, A.; Sörgel, T. Nickel/sulfur composite electroplated nickel foams for the use as 3D cathode in lithium/sulfur batteries—A proof of concept. *Energy Storage Mater.* **2018**, *10*, 223–232.

[25] Chi, S. S.; Liu, Y. C.; Song, W. L.; Fan, L. Z.; Zhang, Q. Prestoring lithium into stable 3D nickel foam host as dendrite-free lithium metal anode. *Adv. Funct. Mater.* **2017**, *27*, 1700348.

[26] Yu, X. L.; Deng, J. J.; Lv, R. T.; Huang, Z. H.; Li, B. H.; Kang, F. Y. A compact 3D interconnected sulfur cathode for high-energy, high-power and long-life lithium–sulfur batteries. *Energy Storage Mater.* **2019**, *20*, 14–23.

[27] Xiang, Y. Y.; Lu, L. Q.; Kottapalli, A. G. P.; Pei, Y. T. Status and perspectives of hierarchical porous carbon materials in terms of high-performance lithium–sulfur batteries. *Carbon Energy* **2022**, *4*, 346–398.

[28] Yi, G.; Li, H.; Zang, C. Y.; Xiao, W. L.; Ma, C. L. Remarkable improvement in strength and ductility of Al–Cu foundry alloy by submicron-sized TiC particles. *Mater. Sci. Eng.: A* **2022**, *855*, 143903.

[29] Nie, J. F.; Liu, X. F.; Wu, Y. Y. The influences of B dopant on the crystal structure and nucleation ability of TiC_x in the Al melt. *Mater. Res. Bull.* **2013**, *48*, 1645–1650.

[30] Zhou, L.; Li, Y. Y.; Kou, Z. L.; Zheng, L. P.; Li, Q.; Ma, G. L.; Zhang, Y. J.; He, D. W. Heterogeneous diamond-TiC composites with high fracture toughness and electrical conductivity. *J. Eur. Ceram. Soc.* **2024**, *44*, 4887–4894.

[31] Zhang, Y. S.; Zhang, P.; Zhang, S. J.; Wang, Z.; Li, N.; Silva, S. R. P.; Shao, G. S. A flexible metallic TiC nanofiber/vertical graphene 1D/2D heterostructured as active electrocatalyst for advanced Li–S batteries. *InfoMat* **2021**, *3*, 790–803.

[32] Yi, Q. H.; Dai, X.; Zhao, J.; Sun, Y. H.; Lou, Y. H.; Su, X. D.; Li, Q. W.; Sun, B. Q.; Zheng, H. H.; Shen, M. R. et al. Enhanced mechanical strength and electrical conductivity of carbon-nanotube/TiC hybrid fibers. *Nanoscale* **2013**, *5*, 6923–6927.

[33] Yan, X. B.; Zhang, Y. B.; Wang, Q. Q.; Zhang, X. B.; He, S. P. Wettability between titanium-containing steels and TiC ceramic substrate. *Steel Res. Int.* **2023**, *94*, 2300190.

[34] Ma, T. X.; Pan, Y. Z.; Chen, J. Y.; Yan, Z. M.; Chen, B. X.; Zhao, L.; Hu, L. W.; Wen, L. Y.; Hu, M. L. Synthesis of TiC nanotube arrays and their excellent supercapacitor performance. *J. Mater. Chem. A* **2022**, *10*, 9932–9940.

[35] Shi, Y. Y.; Zheng, D. W.; Zhang, X.; Lv, K.; Wang, F. H.; Dong, B. B.; Wang, S. Y.; Yang, C. X.; Li, J. M.; Yang, F. Y. et al. Self-supported ceramic electrode of 1T–2H MoS_2 grown on the TiC membrane for hydrogen production. *Chem. Mater.* **2021**, *33*, 6217–6226.

[36] Peng, H. J.; Zhang, G.; Chen, X.; Zhang, Z. W.; Xu, W. T.; Huang, J. Q.; Zhang, Q. Enhanced electrochemical kinetics on conductive polar mediators for lithium–sulfur batteries. *Angew. Chem., Int. Ed.* **2016**, *55*, 12990–12995.

[37] Zhang, L.; Bi, J. Y.; Liu, T.; Chu, X. R.; Lv, H. J.; Mu, D. B.; Wu, B. R.; Wu, F. TiN/TiC heterostructures embedded with single tungsten atoms enhance polysulfide entrapment and conversion for high-capacity lithium–sulfur battery applications. *Energy Storage Mater.* **2023**, *54*, 410–420.

[38] Liu, H.; Li, Y. F.; Zeng, P.; Yu, H.; Zhou, X.; Chen, M. F.; Miao, C. Q.; Chen, G. R.; Liu, Q. C.; Luo, Z. G. et al. Multiple roles of titanium carbide in performance boosting: Mediator, anchor and electrocatalyst for polysulfides redox regulation. *Chem. Eng. J.* **2021**, *426*, 130744.

[39] Li, Z.; Qi, C. Y.; Chang, Q.; Jin, J.; Lu, Y.; Wen, Z. Y. TiC nanoparticles supported on free-standing carbon nanofibers enabled high-performance Lithium–sulfur batteries. *Compos. Part B: Eng.* **2023**, *257*, 110679.

[40] Ding, W.; Sternhagen, J.; Jaishi, L. R.; Kharel, P.; Xian, X. J. CVD-synthesized titanium carbide nanoflowers as high-performance anodes for sodium-ion batteries. *Nano Lett.* **2024**, *24*, 13324–13332.

[41] Yao, Y.; Huo, K.; Hu, L. B.; Liu, N.; Cha, J. J.; McDowell, M. T.; Chu, P. K.; Cui, Y. Highly conductive, mechanically robust, and electrochemically inactive TiC/C nanofiber scaffold for high-performance silicon anode batteries. *ACS Nano* **2011**, *5*, 8346–8351.

[42] Canovic, S.; Ljungberg, B.; Halvarsson, M. CVD TiC/alumina multilayer coatings grown on sapphire single crystals. *Micron* **2011**, *42*, 808–818.

[43] Noel, M. S.; Kovar, D. Laser chemical vapor deposition of TiC on tantalum. *J. Mater. Sci.* **2002**, *37*, 689–697.

[44] Kim, Y. J.; Chung, H.; Kang, S. J. L. *In situ* formation of titanium carbide in titanium powder compacts by gas–solid reaction. *Compos. Part A: Appl. Sci. Manuf.* **2001**, *32*, 731–738.

[45] Shah, S. A.; Habib, T.; Gao, H.; Gao, P.; Sun, W.; Green, M. J.; Radovic, M. Template-free 3D titanium carbide ($Ti_3C_2T_x$) MXene particles crumpled by capillary forces. *Chem. Commun.* **2017**, *53*, 400–403.

[46] Yao, S. Y.; Ma, Y. J.; Xu, T. H.; Wang, Z. Y.; Lv, P.; Zheng, J. J.; Ma, C.; Yu, K. H.; Wei, W.; Ostrikov, K. Ti–C bonds reinforced TiO_2@C nanocomposite Na-ion battery electrodes by fluidized-bed plasma-enhanced chemical vapor deposition. *Carbon* **2021**, *171*, 524–531.

[47] Roy, A.; Mukhopadhyay, A. K.; Gupta, M.; Majumdar, A. Negative capacitance effect of Cu–TiC thin film deposited by DC magnetron plasma. *Bull. Mater. Sci.* **2020**, *43*, 260.

[48] Ma, L. R.; Sui, S.; Zhai, Y. C. Preparation and characterization of Ir/TiC catalyst for oxygen evolution. *J. Power Sources* **2008**, *177*, 470–477.

[49] Choi, S. W.; Lee, D. H.; Kim, J.; Kim, J.; Park, J. H.; Beum, H. T.; Lim, D. S.; Lee, K. B. A titanium carbide-derived novel tetrafluoromethane adsorbent with outstanding adsorption performance. *Chem. Eng. J.* **2017**, *311*, 227–235.

[50] Chung, S. H.; Manthiram, A. Current status and future prospects of metal–sulfur batteries. *Adv. Mater.* **2019**, *31*, 1901125.

[51] Xin, S. S.; Li, J.; Cui, H. T.; Liu, Y. Y.; Wei, H. Y.; Zhong, Y. Y.; Wang, M. R. Self-templating synthesis of prismatic-like N-doped carbon tubes embedded with Fe_3O_4 as a high-efficiency polysulfide-anchoring-conversion mediator for high performance lithium–sulfur batteries. *Chem. Eng. J.* **2021**, *410*, 128153.